This article was downloaded by: [University of Illinois at Urbana-Champaign]
On: 20 May 2015, At: 02:30
Publisher: Taylor & Francis
Informa Ltd Registered in England and Wales Registered Number: 1072954 Registered office: Mortimer House, 37-41 Mortimer Street, London W1T 3JH, UK

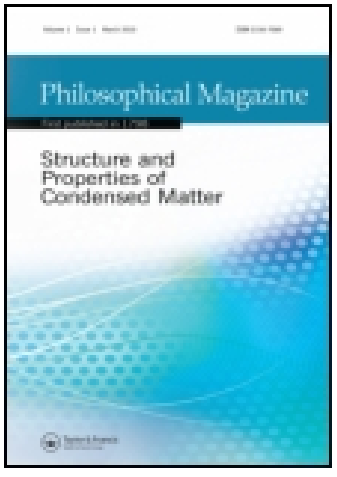

Philosophical Magazine
Publication details, including instructions for authors and subscription information:
http://www.tandfonline.com/loi/tphm20

Modelling of martensite slip and twinning in NiTiHf shape memory alloys

J. Wang[a] & H. Sehitoglu[a]
[a] Department of Mechanical Science and Engineering, University of Illinois at Urbana-Champaign, 1206 W. Green St., Urbana, IL 61801, USA
Published online: 19 May 2014.

CrossMark
Click for updates

To cite this article: J. Wang & H. Sehitoglu (2014) Modelling of martensite slip and twinning in NiTiHf shape memory alloys, Philosophical Magazine, 94:20, 2297-2317, DOI: 10.1080/14786435.2014.913109

To link to this article: http://dx.doi.org/10.1080/14786435.2014.913109

PLEASE SCROLL DOWN FOR ARTICLE

Taylor & Francis makes every effort to ensure the accuracy of all the information (the "Content") contained in the publications on our platform. However, Taylor & Francis, our agents, and our licensors make no representations or warranties whatsoever as to the accuracy, completeness, or suitability for any purpose of the Content. Any opinions and views expressed in this publication are the opinions and views of the authors, and are not the views of or endorsed by Taylor & Francis. The accuracy of the Content should not be relied upon and should be independently verified with primary sources of information. Taylor and Francis shall not be liable for any losses, actions, claims, proceedings, demands, costs, expenses, damages, and other liabilities whatsoever or howsoever caused arising directly or indirectly in connection with, in relation to or arising out of the use of the Content.

This article may be used for research, teaching, and private study purposes. Any substantial or systematic reproduction, redistribution, reselling, loan, sub-licensing, systematic supply, or distribution in any form to anyone is expressly forbidden. Terms &

Conditions of access and use can be found at http://www.tandfonline.com/page/terms-and-conditions

Downloaded by [University of Illinois at Urbana-Champaign] at 02:30 20 May 2015

Philosophical Magazine, 2014
Vol. 94, No. 20, 2297–2317, http://dx.doi.org/10.1080/14786435.2014.913109

Taylor & Francis
Taylor & Francis Group

Modelling of martensite slip and twinning in NiTiHf shape memory alloys

J. Wang and H. Sehitoglu*

Department of Mechanical Science and Engineering, University of Illinois at Urbana-Champaign, 1206 W. Green St., Urbana, IL 61801, USA

(*Received 16 November 2013; accepted 31 March 2014*)

High-temperature shape memory alloy NiTiHf holds considerable promise for structural applications. An important consideration for these advanced alloys is the determination of the magnitude of the twinning stress. Theoretical stresses for twinning and dislocation slip in NiTiHf martensites are determined. The slip and twinning planes are (0 0 1) and (0 1 1) for monoclinic and orthorhombic crystals, respectively. The determination of the slip and twinning stress is achieved with a proposed Peierls–Nabarro-based formulation informed with atomistic simulations. In the case of the twin, multiple dislocations comprising the twin nucleus are considered. The overall energy expression is minimized to obtain the twinning and slip stresses. The magnitude of the predicted twinning stresses is lower than slip stresses which explains why the NiTiHf alloys can undergo reversibility without plastic deformation. In fact, the predicted critical resolved shear stress levels of 433 MPa for slip and 236 MPa for twinning in the case of 12.5% Hf agree very well with the experimental measurements. The high slip resistance confirms that these materials can be very attractive in load-bearing applications.

Keywords: shape memory materials; simulation; twinning; stresses; alloys; atomistic simulation

Downloaded by [University of Illinois at Urbana-Champaign] at 02:30 20 May 2015

1. Introduction

Recently, there has been significant emphasis on high-temperature shape memory alloys [1–7] with potential industrial applications. The major impetus for these developments is that the use of NiTi above 100 °C is limited because of low slip resistance and irrecoverability [1,8]. We note that the martensitic transformation stress for NiTi increases rapidly with increasing temperature, while the dislocation slip stress decreases gradually with increasing temperature. For NiTi at temperatures above 100 °C, the lowering of the slip stress and other recovery mechanisms can induce plastic deformation. For the NiTiHf alloys, the slip strength remains at a high level well beyond 100 °C [6]. One of the most promising among the high-temperature shape memory materials is NiTi with ternary Hf additions [4,9–11]. The widespread utilization of NiTiHf is limited primarily due to the lack of understanding of their shape memory response. There is a correlation between composition and twin stress which needs to be established. The change in composition also changes the lattice parameters and elastic constants, the transition from

*Corresponding author. Email: huseyin@illinois.edu

© 2014 Taylor & Francis

B19′ to B19 martensites, and the planar fault energies that control the twinning response [12,13]. These alloys are either in the B19 (orthorhombic) or in the B19′ (monoclinic) state depending on the Hf content. While research has substantially progressed in the shape memory of NiTi, the understanding of the deformation by twinning is still in progress. Crystallographic planes for slip and twinning and atomic movements for simple lattices (such as fcc and bcc) have been established previously [14,15], but the energetics of twinning in the orthorhombic and monoclinic crystals is rather complex and not well understood. The atomic positions present shuffles within the lattice. This paper addresses the determination of twinning stress and slip stress for NiTiHf alloys.

The deformation behaviour of monoclinic and orthorhombic martensites in NiTi-based shape memory alloys have been studied experimentally [16–20]. The results show that the flow response of the binary NiTi is primarily due to twinning of the monoclinic lattice at rather low stress levels (less than 20 MPa). We note that the strength of NiTi against dislocation slip also depends on the microstructure, the heat-treatment and the precipitate volume fraction [20–23]. It is well known that the addition of ternary elements can also change the mechanical response of NiTi alloys [5,6,11,24]. The relative roles of these hardening mechanisms require further research. The purpose of Hf additions has been to raise the transformation temperatures opening potentially new applications in aerospace industry [6]. As the hafnium content is increased to levels near 25%, the mechanical response such as the slip and twin stress levels should change substantially. The purpose of this paper is to determine the changes in slip stress and twinning stress via modelling without using empirical constants and the results are compared to experiments for cases, where data are available. The methodology developed relies on the generalized stacking fault energy (SFE) (GSFE) [14] for slip and the generalized planar fault energy (GPFE) [15] for twinning.

2. Simulation methods

We performed the first-principles total-energy calculations using the Vienna *ab initio* Simulations Package with the projector augmented wave method and the generalized gradient approximation. In our simulations, Monkhorst–Pack $9 \times 9 \times 9$ k-point meshes were used for the Brillouin-zone integration. Ionic relaxation was applied by a conjugate gradient algorithm and stopped when absolute values of internal forces were smaller than 5×10^{-3} eV/Å. The energy cut-off of 500 eV was used for the plane-wave basis set. The total energy was converged to less than 10^{-5} eV per atom. The energy barriers of dislocation slip and twinning in a crystal are characterized via the GSFE and GPFE curves, respectively. GSFE is the interplanar potential energy determined by rigidly sliding one half of a crystal over the other half. It was first introduced by Vitek [14] and is a comprehensive definition of the fault energy associated with dislocation motion. GPFE provides a comprehensive description of twins, which is the energy per unit area required to form n-layer twins by shearing n consecutive layers along twinning direction. We have used twelve (0 0 1) and (0 1 1) layers in the periodic supercell (no free surfaces) to assess the converged energies in GSFE and GPFE curves. During the shear deformation process, the volume and shape of the supercell were maintained constant, ensuring the correct monoclinic angle and twin/slip structure. In the present study, a full atomic relaxation was carried out, during which atoms can move in the out of plane

Downloaded by [University of Illinois at Urbana-Champaign] at 02:30 20 May 2015

and normal to the slip and twin plane although these displacements are small relative to the shear displacement. This relaxation process caused a small additional atomic displacement $r\left(|r| = \sqrt{r_x^2 + r_y^2 + r_z^2}\right)$ deviating from the Burgers vector. Thus, the total fault displacement is not exactly equal to shear displacement, u, but involves additional r. The total energy of the deformed (faulted) crystal was minimized during this relaxation process through which atoms can avoid coming too close to each other during shear [25,26]. The calculations, involving the displacement in the parallel directions to the twin and slip plane, provided more accurate energy barriers (GSFE and GPFE).

2.1. *Prediction of critical twin nucleation stress by twin nucleation model*

We proposed a twin nucleation model based on Peierls–Nabarro formulation to predict the twinning stress in shape memory alloys (see more details in Ref. [27]). To predict twinning stresses in NiTiHf alloys, we determined the total energy involved in the twin nucleation as follows:

$$\begin{aligned} E_{\text{total}} &= E_{\text{int}} + E_{\text{GPFE}} + E_{\text{line}} - W \\ &= \frac{\mu b^2}{4\pi(1-\nu)}(1-\nu\cos^2\theta)\sum_{m=1}^{N-1}\left(\ln\frac{L}{\sum_{i=1}^{m} d_i} + \ln\frac{L}{\sum_{i=2}^{m} d_i} + \cdots + \ln\frac{L}{\sum_{i=N-1}^{m} d_i}\right) \\ &+ \sum_{m=-\infty}^{+\infty}\gamma_{\text{SF}}[f(mb)]b + (N-1)\sum_{m=-\infty}^{+\infty}\gamma_{\text{twin}}[f(mb)]b + \frac{N\mu b^2}{2(1-\nu)}(1-\nu\cos^2\theta) \\ &- \sum_{i=1}^{N-1}\tau s h d_i, \quad i = 1,2,3,\ldots,N-1, \end{aligned} \tag{1}$$

where, E_{int} is the twin dislocations interaction energy, E_{GPFE} is the twin boundary energy (GPFE), E_{line} is the twin dislocations line energy and W is the applied work; μ is the shear modulus in the twinning system, b is the twinning Burgers vector, ν is the Poisson's ratio, θ is the angle between the Burgers vector and the dislocation line, L is the dimensions of the crystal containing the twin; τ is the applied shear stress and the minimum τ to form a twin is called critical twin nucleation stress, τ_{crit}; N is the number of twin nucleation layers, h is the twin thickness, s is the twinning shear and d_i is the equilibrium spacing between two adjacent twinning dislocations i and $i+1$ corresponding to the minimum total energy.

Figure 1 shows a schematic of twin formation in B19 Ni_2TiHf, where $N=3$ and $i=1, 2$ are determined corresponding to Equation (1).

We minimized the total energy for the twin nucleation, E_{total}, with respect to d_i:

$$\frac{\partial E_{\text{total}}}{\partial d_i} = 0, \quad i = 1,2,3,\ldots,N-1, \tag{2}$$

By numerically solving the above set of $N-1$ equations, the critical twinning stress can be determined as the minimum value of the applied stress, where these equations satisfy. We note that all parameters involved in Equations (1) and (2) can be calculated from atomistic simulations, and no fitting parameter from experimental measurements is needed.

Downloaded by [University of Illinois at Urbana-Champaign] at 02:30 20 May 2015

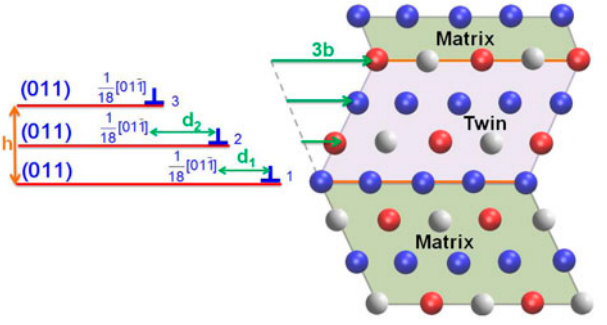

Figure 1. (colour online) Schematic of three-layer twin formation in B19 Ni_2TiHf. The twin plane is (0 1 1) and twinning Burgers vector is $\frac{1}{18}[0\,1\,\bar{1}]$; h is the twin thickness and d_i is the equilibrium spacing between two adjacent twinning dislocations i and $i+1$ corresponding to the minimum total energy. For the case of twin nucleation of B19 Ni_2TiHf, we have $i = 1, 2$.

2.2. *Prediction of Peierls stress for dislocation slip by extended P–N model*

We extended the Peierls–Nabarro model to predict the slip stress (Peierls stress) in shape memory alloys (see more details in Ref. [28]). To calculate the Peierls stress, τ_p, for dislocation slip in NiTiHf alloys, we determined the misfit energy $E_\gamma(u)$ with the obtained dislocation profiles, which depends on the position of the dislocation line within a lattice and reflects the lattice periodicity [29]. To consider the discreteness of the crystal in the slip plane, the $E_\gamma(u)$ is obtained as the sum of all the misfit energies between pairs of atomic planes and can be calculated from the GSFE:

$$E_\gamma(u) = \sum_{m=-\infty}^{+\infty} \gamma[f(ma' - u)]a' \tag{3}$$

where $\gamma[f(x)]$ is obtained from the GSFE curve from the first-principles calculations, a' is the periodicity of E_γ and is the distance between adjacent atomic planes along the

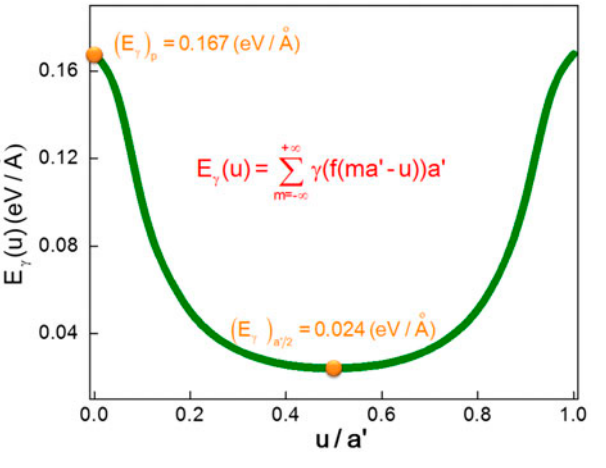

Figure 2. (colour online) Misfit energy $E_\gamma(u)$ for the dislocation $(0\,1\,1)[0\,1\,\bar{1}]$ of B19 Ni_2TiHf.

Downloaded by [University of Illinois at Urbana-Champaign] at 02:30 20 May 2015

direction perpendicular to the dislocation line; $f(x)$ is the dislocation profile (disregistry function) determined from the relative displacement of two half crystals in the slip plane along x direction [30], and u is the position of dislocation line.

Figure 2 shows the misfit energy $E_\gamma(u)$ variation with the lattice period a' for the $(0\,1\,1)[0\,1\,\bar{1}]$ slip of B19 Ni_2TiHf. The Peierls stress τ_p can be calculated by the maximum of $\frac{1}{b}\frac{dE^s_\gamma(u)}{du}$. In the misfit energy curve, $(E^s_\gamma)_{a'/2}$ is the minimum value of $E^s_\gamma(u)$ and provides an estimate of the core energy of dislocations; $(E^s_\gamma)_p$, defined as the Peierls energy, is the barrier required to move dislocations.

3. Results

In this paper, we studied martensitic phase Ni_4Ti_3Hf ($Ni_{50}Ti_{37.5}Hf_{12.5}$) and Ni_2TiHf ($Ni_{50}Ti_{25}Hf_{25}$) alloys including the determination of crystal structure, prediction of slip and twin nucleation stresses (Section 3.1) in Tables 1 and 2. We compared the results to B19′ NiTi to show the stress change by adding ternary addition Hf to NiTi. Table 1 shows the calculated lattice parameters for B19′ Ni_4Ti_3Hf and B19 Ni_2TiHf, which are monoclinic and orthorhombic structures, respectively. The results are well comparable to the available experimental data, which form the foundation of atomistic simulations in the present study. Table 2 shows the calculated energy associated to dislocation slip (GSFE) and twin (GPFE), and the predicted slip and twinning stresses in martensitic NiTiHf. The slip and twinning stresses for B19′ NiTi are also calculated and compared to those of NiTiHf alloys. The calculated results are compared to experiments for cases where data is available. The good agreement between them validates the prediction from our models.

We plot the predicted dislocation slip and twinning stresses of $Ni_{50}Ti_{(50-x)}Hf_x$ alloys variation with the composition x in Figure 3. The composition x is the concentration of Hf in $Ni_{50}Ti_{(50-x)}Hf_x$ ($x=0$, NiTi; $x=6.25$, Ni_8Ti_7Hf; $x=12.5$, Ni_4Ti_3Hf; $x=25$, Ni_2TiHf). In this figure, we also included the prediction of slip and twinning stresses in

Table 1. Calculated lattice parameters are compared to available experimental data in NiTiHf alloys. For comparison, previous calculated lattice parameters of NiTi are also given.

	Lattice parameter (Å)	
Material (Structure)	This study	Experiments
NiTi (monoclinic- B19′)	$a=2.88$, $b=4.11$, $c=4.66$, $\gamma=97.8^\circ$ [31]	$a=2.90$, $b=4.11$, $c=4.65$, $\gamma=97.8^\circ$ [32]
Ni_8Ti_7Hf (monoclinic- B19′)	$a=2.89$, $b=4.13$, $c=4.70$, $\gamma=98.4^\circ$	$a=2.85$, $b=4.15$, $c=4.67$, $\gamma=98.3°$[13]
Ni_4Ti_3Hf (monoclinic- B19′)	$a=2.97$, $b=4.06$, $c=4.77$, $\gamma=98.9^\circ$	$a=2.95$, $b=4.11$, $c=4.75$, $\gamma=99.0°$[13]
Ni_2TiHf (orthorhombic-B19)	$a=3.02$, $b=4.20$, $c=4.69$	–

Note: The dash indicates that experimental data were not available for comparison.

Downloaded by [University of Illinois at Urbana-Champaign] at 02:30 20 May 2015

Downloaded by [University of Illinois at Urbana-Champaign] at 02:30 20 May 2015

Table 2. Calculated energies associated to dislocation slip (GSFE) and twinning (GPFE), slip and twinning stress are compared to available experimental data in NiTi and NiTiHf alloys.

Material (Structure)	Slip system Burgers vector (Å)	GSFE (Slip) (mJ/m^2)		Slip stress (MPa)		Twin system Burgers vector (Å)	GPFE (Twin) (mJ/m^2)		Twinning stress (MPa)	
		γ_{us}	γ_{isf}	This study	Experiments		γ_{ut}	$2\gamma_{tsf}$	This study	Experiments
NiTi (monoclinic- B19′)	(0 0 1)[1 0 0] $b = 1.442$	20 [31]	9 [31]	36	–	(0 0 1)[1 0 0] b=1.442	25 [31]	17 [31]	20 [27]	20–28 [19,31]
Ni_8Ti_7Hf (monoclinic- B19′)	(0 0 1)[1 0 0] $b = 1.445$	174	33	286	–	(0 0 1)[1 0 0] $b = 1.445$	148	35	161	180 [33]
Ni_4Ti_3Hf (monoclinic- B19′)	(0 0 1)[1 0 0] $b = 1.49$	271	49	433	350–500 [6]	(0 0 1)[1 0 0] $b = 1.49$	199	103	236	200–275 [34,35]
Ni_2TiHf (orthorhombic- B19)	(0 0 1)[1 0 0] $b = 3.02$	489	–	556	–	(0 1 1)[0 $\bar{1}$ 1] $b = 0.35$	203	158	291	–
	(0 1 1)[0 $\bar{1}$ 1] $b = 3.15$	1770	205	2083	–					

Note: The dash indicates that experimental data were not available for comparison. The slip and twin stresses are shaded grey for clarity.

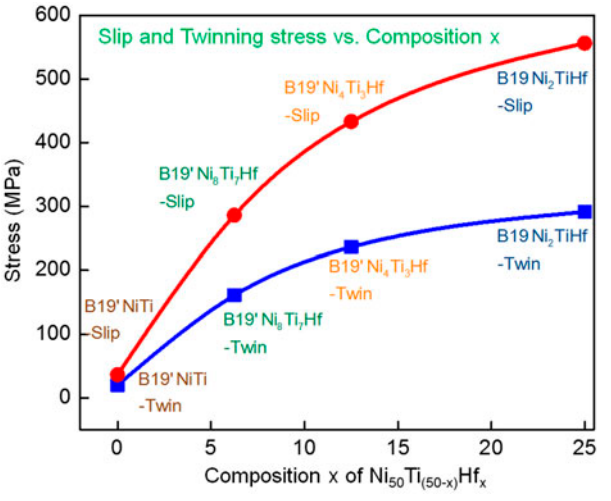

Figure 3. (colour online) Predicted dislocation slip and twinning stress in the martensite phase of $Ni_{50}Ti_{(50-x)}Hf_x$ alloys, variation with composition x ($x = 0$, NiTi; $x = 6.25$, Ni_8Ti_7Hf; $x = 12.5$, Ni_4Ti_3Hf; $x = 25$, Ni_2TiHf). The stress values are given in Table 2.

Ni_8Ti_7Hf ($Ni_{50}Ti_{43.75}Hf_{6.25}$). We note that for all these alloys, the twinning stress (blue square) is lower than slip stress (red circle), which indicates that twinning is more favourable than dislocation slip as the deformation mechanism. However, the dislocation slip can also be activated at high local stress. Furthermore, we note that both slip and twinning stresses increase as composition x becomes larger, especially for slip stress. This indicates that the ternary addition of Hf can significantly increase the strength in martensite NiTi and thus results in fully recoverable shape memory behaviour under high stress levels.

3.1. *Results of B19′ Ni_4Ti_3Hf*

In Ni_4Ti_3Hf, the martensitic phase B19′ has a monoclinic structure and can be described in terms of three lattice parameters a, b, c and a monoclinic angle γ. Figure 4 shows the crystal structure of B19′ Ni_4Ti_3Hf and its view from the [0 1 0] direction. The supercell consists of two B19′ subcells with total eight atoms in an atomic ratio of 4:3:1. The lattice parameters a, b, c and monoclinic angle γ used in GSFE and GPFE calculations are given in Table 1. Here, the c-axis is the longest axis and the a-axis is the shortest one, while the b-axis is the intermediate. The monoclinic angle γ is between the [1 0 0] and [0 0 1] directions.

Similar to the case of martensitic B19′ NiTi [32,36,37], the (0 0 1)[1 0 0] system for dislocation slip and twin was also experimentally observed to be the dominant defect in B19′ NiTiHf alloys [9,38,39]. The slip and twin plane (0 0 1) is shown in a shaded red, and the slip and twin direction [1 0 0] is shown in a red arrow in Figure 4(a).

Downloaded by [University of Illinois at Urbana-Champaign] at 02:30 20 May 2015

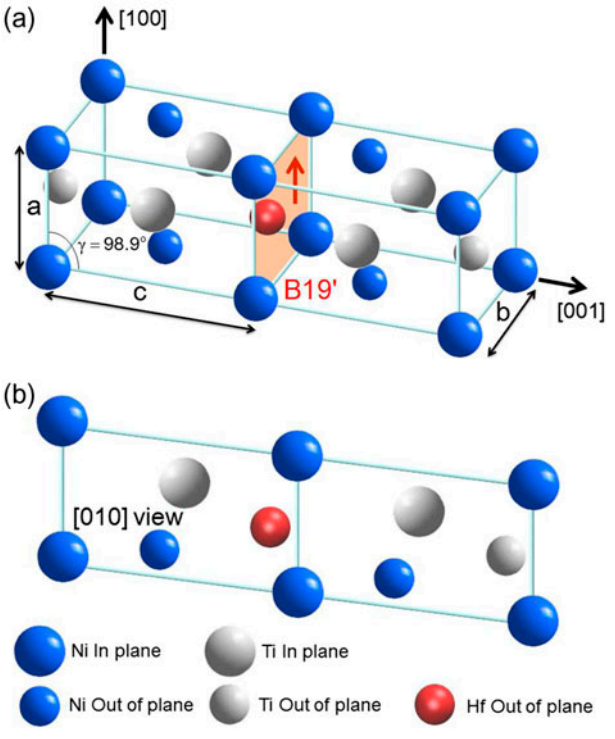

Figure 4. (colour online) (a) Crystal structure of martensite B19′ Ni_4Ti_3Hf ($Ni_{50}Ti_{37.5}Hf_{12.5}$). The supercell consists of two B19′ subcells with total eight atoms in an atomic ratio of 4:3:1. The slip and twin plane (0 0 1) is shown in shaded red, and the slip and twin direction [1 0 0] is shown in a red arrow. Lattice parameters a, b, c and monoclinic angle γ are given in Table 1. The blue, grey and red atoms represent Ni, Ti and Hf, respectively. The different size of atoms indicates that atoms are in plane and out of plane. (b) The [0 1 0] view of B19′ Ni_4Ti_3Hf.

3.1.1. *(0 0 1)[1 0 0] twinning of B19′ Ni_4Ti_3Hf*

Figure 5(a) shows the perfect lattice of B19′ Ni_4Ti_3Hf, while Figure 5(b) is the lattice with a two-layer twin after shearing 2b (shown in a brown arrow) along the [1 0 0] direction in the (0 0 1) twin plane (marked with a red line). The atomic arrangement is viewed from the [0 1 0] direction. Similar to the (0 0 1)[1 0 0] twinning in B19′ NiTi, two (0 0 1) layers of atoms glide simultaneously when a shear is applied in the [1 0 0] direction [31,32].

We calculated the GPFE curve of the B19′ Ni_4Ti_3Hf by successive shear of every two (1 1 1) layers over $\frac{1}{2}[1\,0\,0]$ twinning dislocation (twinning Burgers vector $b = \frac{a}{2} = 1.485$ Å). The calculated energy landscape (GPFE) for a three-layer twin formation in B19′ Ni_4Ti_3Hf is shown in Figure 6. In the GPFE curve, γ_{us} is defined as the stacking fault nucleation barriers, which is the barrier required to emit the first-layer twinning partial, γ_{isf} as the first-layer intrinsic SFE, γ_{uf} as the twin nucleation barrier, which is the barrier against a one-layer partial fault becoming a two-layer partial fault and $2\gamma_{tsf}$ as twice the twin SFE [27]. These calculated fault energies associated to the

Downloaded by [University of Illinois at Urbana-Champaign] at 02:30 20 May 2015

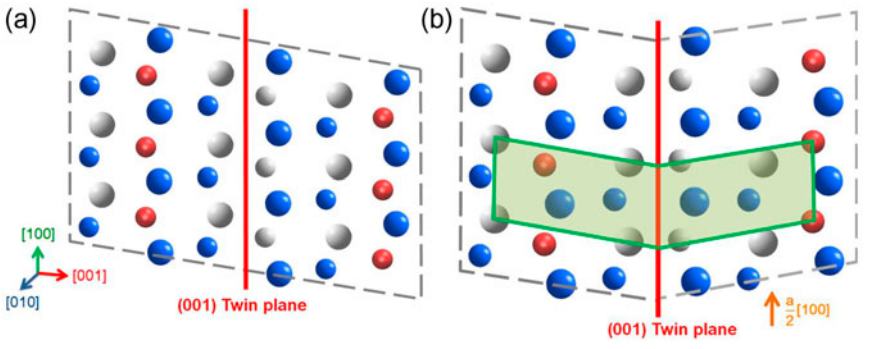

Figure 5. (colour online) Schematic of twinning in the (0 0 1) plane with twinning dislocation $\frac{1}{2}[1\,0\,0]$ of *B19′* Ni_4Ti_3Hf. (a) The perfect B19′ lattice observed from the [0 1 0] direction. The twin plane (0 0 1) is marked with a red line. (b) The lattice with a two-layer twin after shearing along $\frac{1}{2}[1\,0\,0]$ shown in a brown arrow.

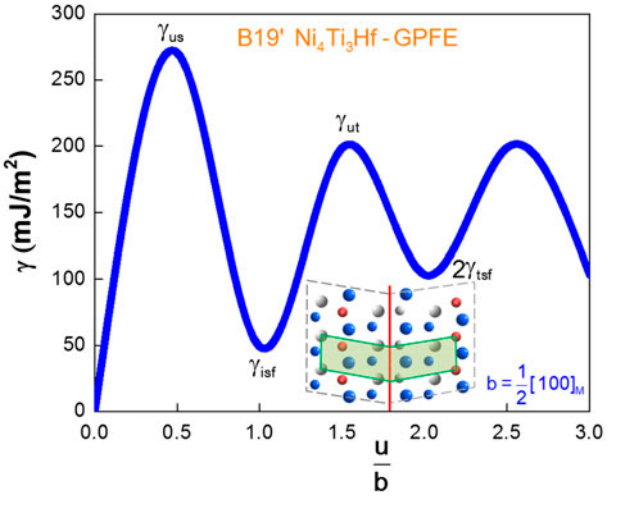

Figure 6. (colour online) The GPFE curve in the twin plane (0 0 1) with twin dislocation $\frac{1}{2}[1\,0\,0]$ of B19′ Ni_4Ti_3Hf. The shear displacement, u, is normalized by the twinning Burgers vector $b = \frac{a}{2} = 1.485$ Å. The calculated fault energies are given in Table 2.

twin process are given in Table 2. The critical twin nucleation stress of B19′ Ni_4Ti_3Hf is calculated as 236 MPa utilizing our developed twin nucleation model.

3.1.2. *(0 0 1)[1 0 0] slip of B19′ Ni_4Ti_3Hf*

The (0 0 1)[1 0 0] slip of B19′ Ni_4Ti_3Hf is illustrated in Figure 7 showing the configuration of slip in the plane (0 0 1) with the dislocation $\frac{1}{2}[1\,0\,0]$. Figure 5(a) is the perfect B19′ lattice before shear, while Figure 7(b) is the lattice after shear by one Burgers vector, $b = \frac{a}{2} = 1.485$ Å, in the slip plane. All fault energies computed as a function of shear displacement, u, are determined relative to the energy of the undeformed B19′.

Downloaded by [University of Illinois at Urbana-Champaign] at 02:30 20 May 2015

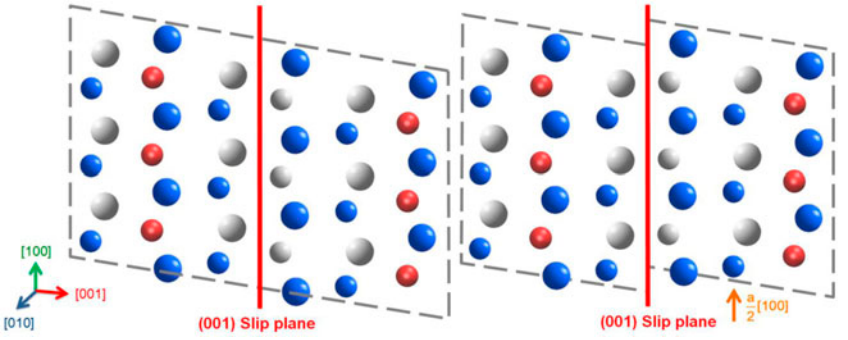

Figure 7. (colour online) Schematic of slip in the (0 0 1) plane with dislocation $\frac{1}{2}[1\,0\,0]$ of B19′ Ni_4Ti_3Hf. (a) The perfect B19′ lattice observed from the [0 1 0] direction. The slip plane (0 0 1) is marked with a red line. (b) The lattice after a rigid shear with dislocation $\frac{1}{2}[1\,0\,0]$ is shown in a brown arrow.

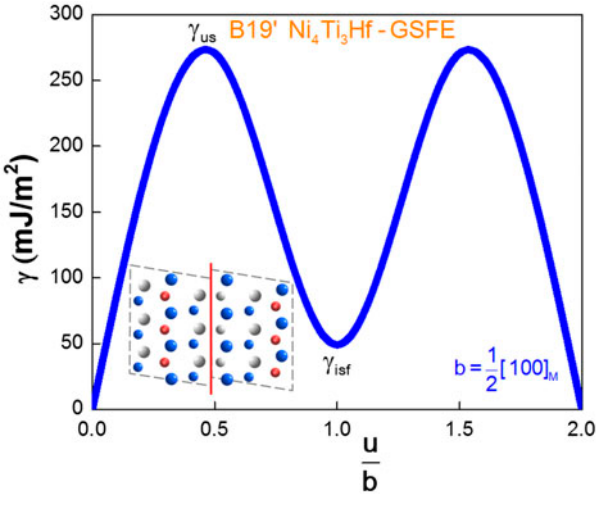

Figure 8. (colour online) The GSFE curve of the slip system (0 0 1)[1 0 0] in B19′ Ni_4Ti_3Hf. The dislocation [1 0 0] can dissociate into two partials $\frac{1}{2}[1\,0\,0]$ connected by a SFE γ_{isf}. The calculated γ_{isf} and unstable SFE γ_{us} are given in Table 2.

The calculated GSFE curve in the slip system (0 0 1)[1 0 0] is shown in Figure 8. The metastable position is indicated as γ_{isf} after shear of one Burgers vector, and two unstable energy barriers for slip are calculated in $\frac{b}{2}$ and $\frac{3b}{2}$. This indicates that the dislocation [1 0 0] in the (0 0 1) plane can dissociate into two partial dislocations as follows:

$$[1\,0\,0] = \frac{1}{2}[1\,0\,0] + \frac{1}{2}[1\,0\,0] \tag{4}$$

The calculated fault energies associated to the slip are given in Table 2. The Peierls stress required to move dislocations of B19′ Ni_4Ti_3Hf is calculated as 433 MPa (Table 2) utilizing our extended Peierls–Nabarro model.

Downloaded by [University of Illinois at Urbana-Champaign] at 02:30 20 May 2015

Downloaded by [University of Illinois at Urbana-Champaign] at 02:30 20 May 2015

3.2. *Results of B19 Ni_2TiHf*

The Ni-rich NiTiHf alloys containing higher Hf content have been reported to have B19 orthorhombic martensite phase [4,40], which transforms in a single step from B2 austenite cubic phase. The B19 martensite Ni_2TiHf ($Ni_{50}Ti_{25}Hf_{25}$) can be described in terms of three lattice parameters a, b and c as given in Table 1. Figure 9 shows the crystal structure of martensite B19 Ni_2TiHf ($Ni_{50}Ti_{25}Hf_{25}$) and its view from the [0 1 0] direction. The short brown arrow shows the internal atomic shuffle within the unit cell, which lowers the crystal structural energy.

We note that the internal atomic shuffle in B19 martensite NiTi has been proposed and theoretically investigated [12,41,42], which can lower the structural energy compared to the case without shuffle. Otsuka and Ren [12] proposed a basal shuffle mode $\{1\,1\,0\}\langle 1\,\bar{1}\,0\rangle_{B2}$ in B19 NiTi, i.e. atoms in $\{1\,1\,0\}_{B2}$ plane move in the $\langle 1\,\bar{1}\,0\rangle_{B2}$ direction (the plane and direction are in the B2 lattice coordinate system). Kibey et al. applied this shuffle mode in the energy landscape for the phase transformation from B2 to B19 in NiTi, and their simulation results showed that this atomic shuffle lowered the structural energy of B19 NiTi [43].

On the other hand, Zhong et al. [41] observed another shuffle mode $\{1\,1\,0\}[0\,0\,1]_{B2}$ in NiTi from Molecular Dynamics (MD) simulations, i.e. atoms in $\{1\,1\,0\}_{B2}$ plane move in the $[0\,0\,1]_{B2}$ direction. Their results are consistent with the recent study by Hatcher [42] utilizing first-principle calculations who found that the atomic shuffle on $\{1\,1\,0\}[0\,0\,1]_{B2}$ requires the lowest energy barrier or even no energy barriers during the phase transformation path in NiTi.

To determine which shuffle mode dominates the crystal structure of B19 Ni_2TiHf, we calculated the structural energy by applying the two shuffle modes described above. These modes $\{1\,1\,0\}\langle 1\,\bar{1}\,0\rangle_{B2}$ and $\{1\,1\,0\}[0\,0\,1]_{B2}$ correspond to $(0\,1\,0)[0\,0\,1]_{B19}$ and $(0\,0\,1)[1\,0\,0]_{B19}$ in the B19 lattice coordinate system. There are two noticeable features between the basal shuffle mode in Figure 9 and the one proposed in Figure 10. The shuffle magnitude at the minimum structural energy in the shuffle mode (0 1 0)[0 0 1] was found to be $0.09c = 0.42$ Å, while it was calculated as $0.045a = 0.14$ Å in the shuffle mode (0 0 1)[1 0 0]. This indicates that the movement of atoms in the (0 0 1)

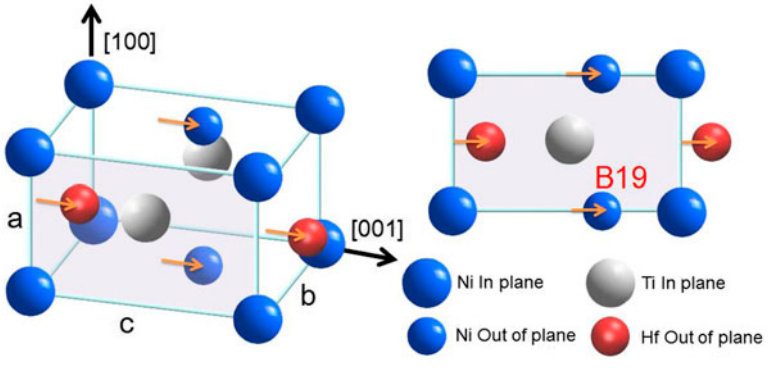

Figure 9. (colour online) The basal shuffle mode (0 1 0)[0 0 1] in B19 Ni_2TiHf, i.e. atoms in (0 1 0) plane move in the [0 0 1] direction.

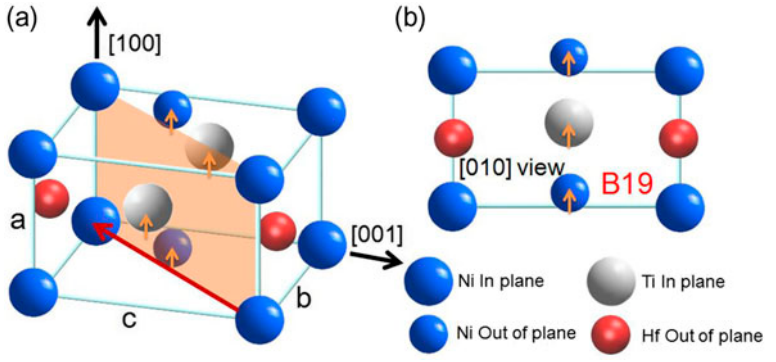

Figure 10. (colour online) (a) Crystal structure of martensite B19 Ni_2TiHf ($Ni_{50}Ti_{25}Hf_{25}$). The twin plane $\{0\,1\,1\}$ is shown in shaded red and the twin direction $\langle 0\,\bar{1}\,1\rangle$ is shown in a red arrow. Lattice parameters a, b and c are given in Table 1. The short brown arrow shows the shuffle mode (0 0 1)[1 0 0] lowering the structure energy. (b) The [0 1 0] view of B19 Ni_2TiHf.

plane along the [1 0 0] direction has shorter shear displacement to obtain the stable position. Additionally, the calculated structural energy in B19 Ni_2TiHf with shuffle mode (0 1 0)[0 0 1] (−30.160 eV/formula unit) is higher than the one with (0 0 1)[1 0 0] (−30.167 eV/formula unit) by 7 meV/formula unit, and thus the shuffle mode (0 1 0)[0 0 1] is not dominant in B19 Ni_2TiHf. Therefore, in the following studies of dislocation slip and twin nucleation in B19 Ni_2TiHf, we established the GSFE and GPFE curves for the B19 structure with shuffle mode $(0\,0\,1)[1\,0\,0]_{B19}$, as it has greater stability.

3.2.1. *(0 1 1)[0 1 $\bar{1}$] twinning of B19 Ni_2TiHf*

The (0 1 1)[0 1 $\bar{1}$] twinning has been observed in B19 orthorhombic structures as the predominant twin type [44–46]. In the present study, the (0 1 1) [0 1 $\bar{1}$] is also considered

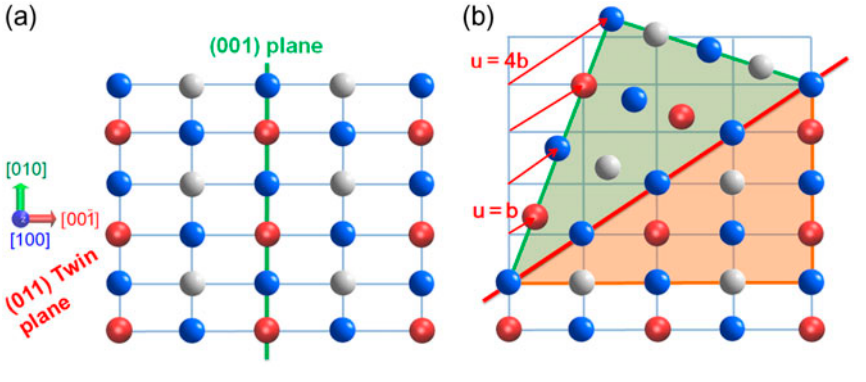

Figure 11. (colour online) Schematic of twinning in the (0 1 1) plane with dislocation [0 1 $\bar{1}$] of B19 Ni_2TiHf. (a) The perfect B19 lattice observed from the [1 0 0] direction. The twin plane (0 1 1) is marked with a red line and the (0 0 1) symmetry plane shown in green line is the plane of symmetry. (b) The lattice with a four-layer twin after shearing 4b ($b = \frac{1}{18}[0\,1\,\bar{1}]$) shown in a red arrow.

Downloaded by [University of Illinois at Urbana-Champaign] at 02:30 20 May 2015

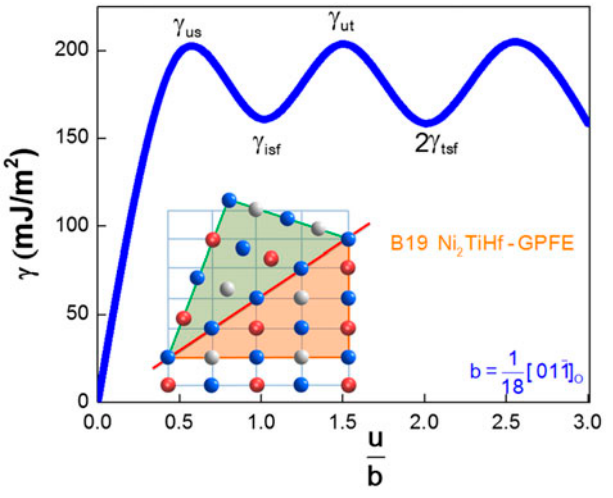

Figure 12. (colour online) The GPFE curve in (0 1 1) twin plane with $[0\,1\,\bar{1}]$ twinning dislocation of B19 Ni_2TiHf. The shear displacement, u, is normalized by the twinning Burgers vector $b = \frac{1}{18}[0\,1\,\bar{1}]$. The calculated fault energies are given in Table 2.

as the twinning system in B19 Ni_2TiHf. Figure 11(a) shows the perfect lattice of B19 Ni_2TiHf, while Figure 11(b) is the lattice with a four-layer twin after shearing 4b (shown in a red arrow) along the $[0\,1\,\bar{1}]$ direction in the (0 1 1) plane (twin plane is marked with a red line). The atomic arrangement is viewed from the [1 0 0] direction. We note that unlike B19′ monoclinic structure, where (0 0 1) plane is a twin plane, the (0 0 1) plane in B19 orthorhombic structure is a plane of symmetry and therefore is not a twin plane [44]. Figure 11(a) shows the (0 0 1) plane (marked in green line) as a plane of symmetry, which will not provide twinning in the orthorhombic unit cell.

We calculated the GPFE curve of B19 Ni_2TiHf by successive shear of every (0 1 1) layer over the twinning dislocation $b = \frac{1}{18}[0\,1\,\bar{1}]$ (twinning Burgers vector $b = 0.35$ Å). The calculated energy landscape for a three-layer twin formation in B19 Ni_2TiHf is shown in Figure 12, and the fault energies associated to the twin process are given in Table 2. The critical twin nucleation stress of B19 Ni_2TiHf is calculated as 296 MPa (Table 2).

3.2.2. *(0 1 1)*$[0\,1\,\bar{1}]$ *slip of B19 Ni_2TiHf*

Both (0 1 1)$[0\,1\,\bar{1}]$ and (0 0 1)[1 0 0] slip systems have been theoretically investigated and experimentally observed in orthorhombic structures [47,48], which will be also considered as slip systems of B19 Ni_2TiHf in the present study. The (0 1 1) $[0\,1\,\bar{1}]$ slip of of B19 Ni_2TiHf is illustrated in Figure 13 showing the configuration of slip in the plane (0 1 1) with dislocation $[0\,1\,\bar{1}]$. Figure 13(a) is the perfect B19 lattice before shear viewed from the [1 0 0] direction, while Figure 13(b) is the lattice after shear by a half Burgers vector $\frac{b}{2}$ ($b = 3.15$ Å) in the slip plane.

The calculated GSFE curve in the slip system (0 1 1)$[0\,1\,\bar{1}]$ of B19 Ni_2TiHf is shown in Figure 14. Similar to the slip of B19′ Ni_4Ti_3Hf, the metastable position is

Downloaded by [University of Illinois at Urbana-Champaign] at 02:30 20 May 2015

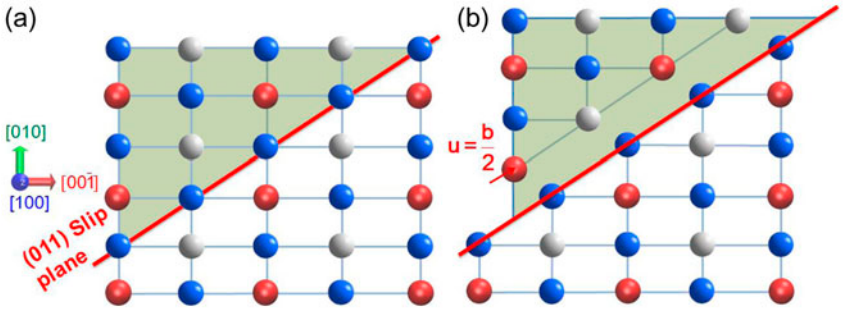

Figure 13. (colour online) Schematic of dislocation slip in the plane (0 1 1) with dislocation $[0\,1\,\bar{1}]$ of B19 Ni_2TiHf. (a) The perfect B19 lattice observed from the [1 0 0] direction. The slip plane (0 1 1) is marked with a red line. (b) The lattice after a rigid shear with displacement $u = \frac{b}{2}$ ($b = \frac{1}{2}[0\,1\,\bar{1}]$) shown in a red arrow.

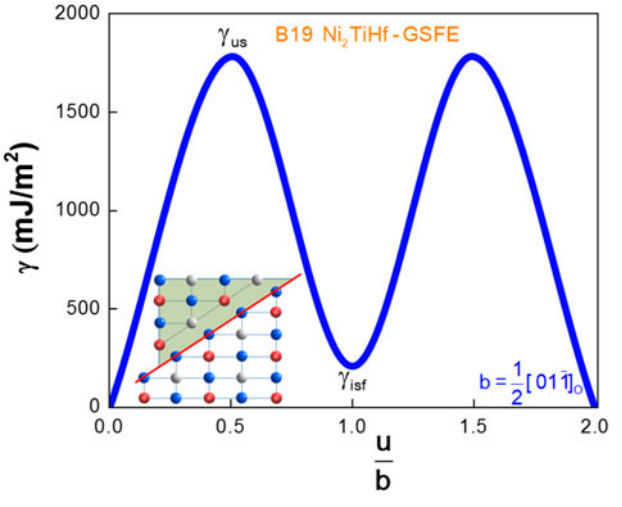

Figure 14. (colour online) The GSFE curve of the slip system $(0\,1\,1)[0\,1\,\bar{1}]$ in B19 Ni_2TiHf. The dislocation $[0\,\bar{1}\,1]$ can dissociate into two partials $\frac{1}{2}[0\,\bar{1}\,1]$ connected by a SFE γ_{isf}. The calculated γ_{isf} and unstable SFE γ_{us} are given in Table 2.

indicated as γ_{isf} after shear one Burgers vector, b, and two unstable energy barriers for slip are found in $\frac{b}{2}$ and $\frac{3b}{2}$. Thus, the $[0\,1\,\bar{1}]$ dislocation in (0 1 1) plane can dissociate into two partial dislocations $\frac{1}{2}[0\,1\,\bar{1}]$ as follows:

$$[0\,1\,\bar{1}] = \frac{1}{2}[0\,1\,\bar{1}] + \frac{1}{2}[0\,1\,\bar{1}] \tag{5}$$

The calculated stacking fault energies are given in Table 2, and the Peierls stress of $(0\,1\,1)[0\,1\,\bar{1}]$ B19 Ni_2TiHf is calculated as 2083 MPa, which is significantly higher than the twinning stress.

Downloaded by [University of Illinois at Urbana-Champaign] at 02:30 20 May 2015

Downloaded by [University of Illinois at Urbana-Champaign] at 02:30 20 May 2015

3.2.3. *(0 0 1)[1 0 0] slip of B19 Ni_2TiHf*

The plane (0 0 1) and direction [1 0 0] were chosen from the family $\{0\,0\,1\}\langle 1\,0\,0\rangle$ as the slip system of B19 Ni_2TiHf, which correspond to the largest interplanar distance (axis c) in $\{0\,0\,1\}$ and the shortest Burgers vector (axis a) in $\langle 1\,0\,0\rangle$. Thus, the slip (0 0 1)[1 0 0] will obtain a lower energy barrier and a smaller required stress compared to other $\{0\,0\,1\}\langle 1\,0\,0\rangle$ systems. Figure 15(a) is the perfect B19 lattice before shear viewed from the $[0\,1\,\bar{1}]$ direction, while Figure 15(b) is the lattice after shear by a half Burgers vector $\frac{b}{2}$ ($b = [1\,0\,0] = 3.02$ Å) in the (0 0 1) slip plane.

The calculated GSFE curve in the slip system (0 0 1)[1 0 0] of B19 Ni_2TiHf is shown in Figure 16. We note that the calculated peak energy barrier, γ_{us}, as 489 mJ/m^2

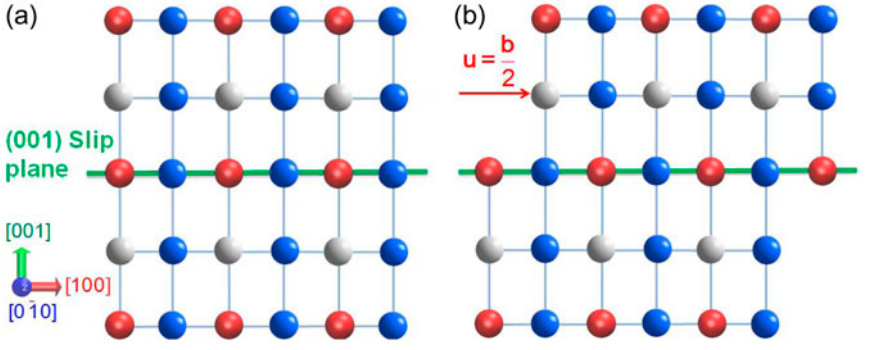

Figure 15. (colour online) Schematic of dislocation slip in the (0 0 1) plane with [1 0 0] dislocation of B19 Ni_2TiHf. (a) The perfect B19 lattice observed from the $[0\,\bar{1}\,0]$ direction The slip plane (0 0 1) is marked with a green line. (b) The lattice after a rigid shear with displacement $u = \frac{b}{2}$ ($b = [1\,0\,0]$) shown in a red arrow.

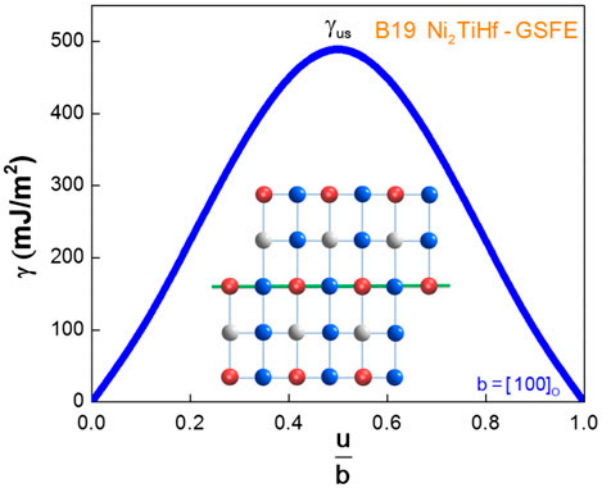

Figure 16. (colour online) The GSFE curve of the slip system (0 0 1)[1 0 0] in B19 Ni_2TiHf. The calculated unstable SFE γ_{us} is given in Table 2.

is much smaller than 1770 mJ/m^2 in the case of (0 1 1)[0 1 $\bar{1}$]. Additionally, unlike the (0 1 1)[0 1 $\bar{1}$] slip there is no metastable energy position in the (0 0 1)[1 0 0] GSFE curve, which prevents the possibility of partial dislocations nucleation in the slip plane along the slip direction. The calculated Peierls stresses of 556 and 2083 MPa for (0 0 1)[1 0 0] and (0 1 1)[0 1 $\bar{1}$] slip indicate that the (0 0 1)[1 0 0] is the most likely slip system of B19 Ni_2TiHf.

4. Discussion and implication of results

The tools to study shape memory alloys have improved along two major fronts in the last two decades. On the theoretical front, the development of atomistic simulations is providing an unprecedented window on the movement of atoms at the crystal level leading to twin formation and the slip behaviour. On the experimental side, there are advances that allow identification of the planes for twinning for example in monoclinic crystals utilizing electron microscopy [31,36,37,49] and more recently neutron diffraction techniques [50]. While the utilization of the experimental tools rely on producing high-quality materials that may be expensive and difficult to make, and the some of the experiments rely on high energy sources that are not easily accessible, the theoretical approaches have the advantages of scoping different compositions and analysing the potential activation of different twinning systems more rapidly. Previous theoretical approaches resulted in very high ideal values for slip and twinning stresses [31]; however, recent studies incorporating dislocations at the mesoscale resulted in stress predictions in the MPa range in very good agreement with experiments [27,28]. The present theoretical calculations achieve stress levels in close agreement with the experiments for the cases where experiments are available. These calculations provide advancement over the empirical methodologies for twinning proposed in the literature. Some of these methodologies utilize the GSFE and GPFE curves but with empirical constants and predict rather high stress levels compared to experiment.

In the present study, we performed a full atomic relaxation to establish the GSFE and GPFE curves in NiTiHf alloys. During the full relaxation, the atoms can move in the out of plane and normal to the slip/twinning plane although these displacements are small relative to the proposed shear displacement. Compared to the calculations without relaxation, the energy barrier and predicted stress by allowing full relaxation can be lower near 10% and closer to experimental results [28]. Thus, the GSFE and GPFE with full atomic relaxation in the paper represent the precise energy barrier in association with the dislocation glide and twinning formation, and further the predicted slip and twinning stresses. In Table 1, we note that the concentration of Hf in $Ni_{50}Ti_{(50-x)}Hf_x$ ($x = 0$, NiTi; $x = 6.25$, Ni_8Ti_7Hf; $x = 12.5$, Ni_4Ti_3Hf; $x = 25$, Ni_2TiHf) changes the lattice parameters and monoclinic angle of NiTiHf. The ternary addition of Hf can significantly increase the strength in binary NiTi alloys. Both twinning an slip stresses increase with Hf increase, but the twinning stress is always lower than the slip stress, and their difference increases as the concentration of Hf becomes larger.

Considerable effort has been devoted to determining the lattice parameters and the crystal types in the martensitic state for NiTiHf alloys in this study, and for NiTi alloys in our previous work [31]. Because the shape memory behaviour (i.e. deformation behaviour in the martensitic state) is governed by the twinning system, the twinning strain and the twinning stress level, it is important to develop a model that accurately

Downloaded by [University of Illinois at Urbana-Champaign] at 02:30 20 May 2015

predicts the twinning stress. One of the most important twinning planes in NiTi B19′ is the (1 0 0) type. At much higher strains, higher twin modes can be activated as shown in earlier studies [31,37]. But these occur at higher stresses and result in partially recoverable strains. For the B19 crystal structure which occurs when the ternary elements exceed approximately 20%, the (0 1 1) plane displays the twinning mirror symmetry, while the (0 0 1) has not been observed in experiments [44]. Therefore, the (0 0 1) and (0 1 1) crystal planes were studied for B19′ and B19, respectively. We note that because the crystal planes differ, the Burgers vectors associated with B19′ and B19 differ considerably as noted in Tables 1 and 2. We note that there are two internal atomic shuffle modes, (0 1 0)[0 0 1] and (0 0 1)[1 0 0], proposed in the B19 orthorhombic NiTi [12,41], and they can lower the structural energy from the first-principles and MD simulations [41,42]. We applied both these shuffle modes within the B19 Ni_2TiHf in our first principle calculations, and found the structural energy involving the shuffle mode (0 0 1)[1 0 0] is lower than the one with the mode (0 1 0)[0 0 1]. Therefore, the shuffle mode (0 0 1)[1 0 0] dominates in the crystal structure of B19 Ni_2TiHf and we established the GSFE and GPFE curves for the structure with this mode as it has greater stability. Additionally, we note that the calculated shuffle magnitude of NiTiHf is 0.42 and 0.14 Å in the shuffle modes (0 1 0)[0 0 1] and (0 0 1)[1 0 0], respectively. These values are different from the corresponding shuffles of 0.46 Å [43] and 0.17 Å [51] for (0 1 0) [0 0 1] and (0 0 1)[1 0 0], respectively, reported for NiTi.

For a crystal structure undergoing plastic deformation, at least five independent slip (or twinning, which forms another plastic deformation mode) systems are needed to accommodate arbitrary deformations [52,53]. We note that for the plastic deformation of B19′ Ni_4Ti_3Hf, there is only one independent slip (twinning) system (0 0 1)[1 0 0] for the family $\{0\,0\,1\}\langle 1\,0\,0\rangle$, since in the low-symmetry monoclinic structure the (0 0 1) plane is different to (1 0 0) and (0 1 0) planes and [1 0 0] direction is different to [0 1 0] and [0 0 1] directions. Therefore, additional independent slip (twinning) systems are required and can be activated at higher applied stresses, such as (1 0 0)[0 0 1], $(2\,0\,\bar{1})[\bar{1}\,0\,\bar{2}]$, $(2\,0\,1)[1\,0\,\bar{2}]$ and $(\bar{1}\,\bar{1}\,3)$ twin, which are also experimentally observed in B19′ NiTi [54]. For the plastic deformation of B19 Ni_2TiHf, we studied two independent slip (twinning) systems (0 0 1)[1 0 0] and $(0\,1\,1)[0\,1\,\bar{1}]$, but $\langle 1\,1\,2\rangle$ twinning [55,56] can be activated at higher stress level to form additional deformation systems.

The design of shape memory alloys requires that the twinning stress remains below the slip stress [27,57]. There is ample demonstration of dislocation generation in shape memory alloys that curtail the reversibility of transformation, produce poor fatigue and shape memory performance [6,23,58–60]. Any attempts to produce alloys that raise the slip resistance without markedly reducing the transformation strain magnitudes are expected to be adopted in structural applications. The NiTi in binary compositions produce large strains and excellent reversibility, and with suitable texturing and ageing treatments can possess higher slip resistance [19,61–63]. The addition of ternary elements give additional freedom in elevating the strength levels. Several ternary additions in NiTi such as Pd, Pt, Cu and Fe have been extensively studied [4,10,42,64–67]. Through the Peierls–Nabarro formulation, we note that the lattice parameters of crystal structure characterize the materials critical stress in slip and twinning. Shearing with a larger Burgers vector requires higher critical stresses [27,68]. For materials having the same slip and twinning systems, the Burgers vector is governed by the lattice parameter. The available experimental data show that the lattice parameter forming the Burgers

Downloaded by [University of Illinois at Urbana-Champaign] at 02:30 20 May 2015

vector in B19′ NiTiPd and B19′ NiTiFe are 2.79 and 2.87 Å, respectively [67]. These values are much smaller than the lattice parameter of 2.97 Å in B19′ NiTiHf. Additionally, we note that among these ternary elements, Hf has the largest atomic radius of 1.55 Å compared to those of Pt (1.35 Å), Pd (1.40 Å), Cu (1.35 Å) and Fe (1.40 Å) [69]. The large atomic radius of Hf results in increase in the Ni–Ni and Ti–Ti bond lengths in the martensite lattice, which is manifested by a higher maximum fault energy and thus higher slip and twinning stresses. Furthermore, ageing the nickel rich $Ni_{50.3}Ti_{29.7}Hf_{20}$ produces a precipitate phase [70] that will increase the slip resistance [71]. However, in the present calculations, we consider stoichiometric compositions and solutionized states. In summary, controlling the plastic deformation and facilitating twinning represents a key in design of advanced shape memory alloys.

5. Conclusions

The work supports the following conclusions:

(1) The fault energies characterizing slip and twinning are elevated with additions of hafnium to NiTi alloy. The corresponding twin and slip stresses are calculated and it is shown that NiTiHf martensites undergo twinning at lower stress levels compared to the slip stresses. Both slip and twinning stresses for martensite NiTiHf increase as the Hf content becomes larger. Compared to the slip stress of 36 MPa in martensitic NiTi, the slip stress in martensite NiTiHf varies from 286 to 556 MPa. The twinning stress in martensite NiTiHf varies from 161 to 291 MPa, which is much higher than the corresponding value of 20 MPa in NiTi.

(2) The precise shuffles within the orthorhombic martensite crystal structures (for 25% Hf case) were established via simulations. Among alternative shuffle arrangements, the one with the lowest energy ([1 0 0] shuffles) was determined and subsequently utilized in the simulations for GSFE and GPFE. As a ternary alloy, NiTiHf has a different atomic arrangement compared to the binary NiTi, and thus its shuffle magnitudes are different than those of NiTi. The shuffle magnitude of NiTiHf is 0.42 Å corresponding to the shuffle mode (0 1 0)[0 0 1], while it is 0.14 Å corresponding to the shuffle mode (0 0 1)[1 0 0]. These values are different from the corresponding shuffles in NiTi of 0.46 Å [43] and 0.17 Å [51] for (0 1 0)[0 0 1] and (0 0 1)[1 0 0], respectively.

(3) Depending on the martensitic structure, the twinning system in NiTiHf can be different. In B19′ monoclinic NiTiHf, the twinning system is (0 0 1)[1 0 0]. However, the (0 0 1) is a plane of symmetry in B19 orthorhombic structure, and thus it is not a twin plane. In B19 orthorhombic NiTiHf, the twinning system is $(0\,1\,1)[0\,1\,\bar{1}]$. In both B19′ and B19 NiTiHf, (0 0 1)[1 0 0] is the slip system.

(4) The calculated energies (GSFE and GPFE) were utilized in a mesoscale model for twinning and slip stress incorporating the Peierls–Nabarro concepts with extensions for group of dislocations. The predicted twinning and slip stresses agree well with the available experiments (within 15% in most cases). Further experiments are needed to study the NiTiHf alloys especially at high Hf concentrations.

Downloaded by [University of Illinois at Urbana-Champaign] at 02:30 20 May 2015

Acknowledgement

This work was supported by the National Science Foundation [CMMI 13-33884], Washington DC, USA.

References

[1] G. Firstov, J. Van Humbeeck and Y.N. Koval, J. Intell. Mater. Syst. Struct. 17 (2006) p.1041.
[2] B. Kockar, I. Karaman, J.I. Kim and Y. Chumlyakov, Scr. Mater. 54 (2006) p.2203.
[3] Y. Chumlyakov, I. Kireeva, E. Panchenko, E. Timofeeva, Z. Pobedennaya, S. Chusov, I. Karaman, H. Maier, E. Cesari and V. Kirillov, Russ. Phys. J. 51 (2008) p.1016.
[4] J. Ma, I. Karaman and R.D. Noebe, Int. Mater. Rev. 55 (2010) p.257.
[5] Y. Tong, Y. Liu and J. Miao, Thin Solid Films 516 (2008) p.5393.
[6] H. Karaca, S. Saghaian, B. Basaran, G. Bigelow, R. Noebe and Y. Chumlyakov, Scr. Mater. 65 (2011) p.577.
[7] L. Kovarik, F. Yang, A. Garg, D. Diercks, M. Kaufman, R. Noebe and M. Mills, Acta Mater. 58 (2010) p.4660.
[8] K. Otsuka and X. Ren, Prog. Mater Sci. 50 (2005) p.511.
[9] X.L. Meng, Y.D. Fu, W. Cai, Q.F. Li and L.C. Zhao, Philos. Mag. Lett. 89 (2009) p.431.
[10] G.S. Bigelow, A. Garg and S.A. Padula II, Scr. Mater. 64 (2011) p.725.
[11] D. Coughlin, P. Phillips, G. Bigelow, A. Garg, R. Noebe and M. Mills, Scr. Mater. (2012) p.112.
[12] K. Otsuka and X. Ren, Mat. Sci. Eng.: A 273–275 (1999) p.89.
[13] M. Zarinejad, Y. Liu and T.J. White, Intermetallics 16 (2008) p.876.
[14] V. Vítek, Philos. Mag. 18 (1968) p.773.
[15] S. Ogata, J. Li and S. Yip, Europhys. Lett. (EPL) 68 (2004) p.405.
[16] S. Rajagopalan, A. Little, M. Bourke and R. Vaidyanathan, Appl. Phys. Lett. 86 (2005) p.081901.
[17] M. Young, M.-X. Wagner, J. Frenzel, W. Schmahl and G. Eggeler, Acta Mater. 58 (2010) p.2344.
[18] S. Qiu, B. Clausen, S. Padula II, R. Noebe and R. Vaidyanathan, Acta Mater. 59 (2011) p.5055.
[19] H. Sehitoglu, I. Karaman, R. Anderson, X. Zhang, K. Gall, H.J. Maier and Y. Chumlyakov, Acta Mater. 48 (2000) p.3311.
[20] R. Delville, B. Malard, J. Pilch, P. Sittner and D. Schryvers, Int. J. Plast. 27 (2011) p.282.
[21] C. Greiner, S.M. Oppenheimer and D.C. Dunand, Acta Biomater. 1 (2005) p.705.
[22] K. Gall, J. Tyber, G. Wilkesanders, S.W. Robertson, R.O. Ritchie and H.J. Maier, Mat. Sci. Eng.: A 486 (2008) p.389.
[23] D.M. Norfleet, P.M. Sarosi, S. Manchiraju, M.F.X. Wagner, M.D. Uchic, P.M. Anderson and M.J. Mills, Acta Mater. 57 (2009) p.3549.
[24] P. Šesták, M. Černý and J. Pokluda, *Influence of comp ound twinning on Young's moduli in NiTi martensite*, in *European Symposium on Martensitic Transformations*, EDP Sciences, Prague, 2009, p.06039.
[25] V. Paidar, Czech. J. Phys. 26 (1976) p.865.
[26] Y.-M. Juan and E. Kaxiras, Philos. Mag. a 74 (1996) p.1367.
[27] J. Wang and H. Sehitoglu, Acta Mater. 61 (2013) p.6790.
[28] J. Wang, H. Sehitoglu and H.J. Maier, Int. J. Plast. 54 (2014) p.247.
[29] B. Joós, Q. Ren and M.S. Duesbery, Phys. Rev. B 50 (1994) p.5890.
[30] L. Lejček, Czech. J. Phys. 23 (1973) p.176.
[31] T. Ezaz, H. Sehitoglu and H.J. Maier, Acta Mater. 59 (2011) p.5893.

Downloaded by [University of Illinois at Urbana-Champaign] at 02:30 20 May 2015

[32] Y. Kudoh, M. Tokonami, S. Miyazaki and K. Otsuka, Acta Metall. 33 (1985) p.2049.
[33] F. Dalle, E. Perrin, P. Vermaut, M. Masse and R. Portier, Acta Mater. 50 (2002) p.3557.
[34] Y. Wang, Y. Zheng, W. Cai and L. Zhao, Scr. Mater. 40 (1999) p.1327.
[35] R. Noebe, T. Biles and S. Padula, Mater. Eng.-New York 32 (2006) p.145.
[36] M. Nishida, S. Ii, K. Kitamura, T. Furukawa, A. Chiba, T. Hara and K. Hiraga, Scr. Mater. 39 (1998) p.1749.
[37] T. Onda, Y. Bando, T. Ohba and K. Otsuka, Mater. Trans., JIM 33 (1992) p.354.
[38] F. Dalle, E. Perrin, P. Vermaut, M. Masse and R. Portier, Acta Mater. 50 (2002) p.3557.
[39] Y. Zheng, W. Cai, J. Zhang, Y. Wang, L. Zhao and H. Ye, Mater. Lett. 36 (1998) p.142.
[40] G.S. Ded, Characterization of Ni-rich NiTiHf based high temperature shape memory alloys, Master's thesis, University of Kentucky, 2010.
[41] Y. Zhong, K. Gall and T. Zhu, Acta Mater. 60 (2012) p.6301.
[42] N.B. Hatcher, Electronic and phononic origins of martensitic behavior in NiTi-based binary and ternary shape memory alloys, Ph.D thesis, Northwestern University, 2010.
[43] S. Kibey, H. Sehitoglu and D.D. Johnson, Acta Mater. 57 (2009) p.1624.
[44] W. Moberly, J. Proft, T. Duerig and R. Sinclair, *Twinless Martensite in TiNiCu Shape Memory Alloys*, in Mater. Sci. Forum, 1989, p.605.
[45] S. Banerjee and P. Mukhopadhyay, *Phase Transformations: Examples from Titanium and Zirconium Alloys*, Vol. 12, Elsevier Science, Jordanhill, 2010.
[46] M. Sarikaya, R. Kikuchi and I.A. Aksay, Physica C 152 (1988) p.161.
[47] D. Banerjee, R. Rowe and E. Hall, *Deformation of the Orthorhombic Phase in Ti–Al–Nb Alloys*, in *MRS Proceedings*, Cambridge University Press, Boston, 1990.
[48] J.P. Poirier, J. Geophys. Res. 80 (1975) p.4059.
[49] M. Nishida, H. Ohgi, I. Itai, A. Chiba and K. Yamauchi, Acta Metall. Mater. 43 (1995) p.1219.
[50] O. Benafan, S.A. Padula, R.D. Noebe, D.W. Brown, B. Clausen and R. Vaidyanathan, Acta Mater. 61 (2013) p.3585.
[51] D. Mutter and P. Nielaba, Phys. Rev. B 82 (2010) p.224201.
[52] G.I. Taylor, Proc. R. Soc. A 145 (1934) p.362.
[53] G.W. Groves and A. Kelly, Philos. Mag. 8 (1963) p.877.
[54] J.X. Zhang, M. Sato and A. Ishida, Acta Mater. 54 (2006) p.1185.
[55] Y. Wang, F. Guyot, A. Yeganeh-Haeri and R.C. Liebermann, Science 248 (1990) p.468.
[56] N. Otani, Y. Funatsu, S. Ichinose, S. Miyazaki and K. Otsuka, Scr. Metall. 17 (1983) p.745.
[57] V. Novák, P. Šittner, J. Pilch and R. Delville, *Effect of Plastic Slip on Thermomechanical Behavior of NiTi polycrystals investigated by micromechanics modelling*, in *European Symposium on Martensitic Transformations*, EDP Sciences, 2009, p.03009.
[58] C. Efstathiou, H. Sehitoglu, P. Kurath, S. Foletti and P. Davoli, Scr. Mater. 57 (2007) p.409.
[59] H. Sehitoglu, J. Wang and H.J. Maier, Int. J. Plast. 39 (2012) p.61.
[60] S. Robertson, A. Pelton and R. Ritchie, Int. Mater. Rev. 57 (2012) p.1.
[61] H. Sehitoglu, J. Jun, X. Zhang, I. Karaman, Y. Chumlyakov, H.J. Maier and K. Gall, Acta Mater. 49 (2001) p.3609.
[62] K. Otsuka and C.M. Wayman, eds., *Shape Memory Materials*, Cambridge University Press, Cambridge, 1998.
[63] Y. Liu, Z. Xie, J. Van Humbeeck and L. Delaey, Acta Mater. 46 (1998) p.4325.
[64] T. Kotil, H. Sehitoglu, H. Maier and Y. Chumlyakov, Mater. Sci. Eng.: A 359 (2003) p.280.
[65] H. Sehitoglu, I. Karaman, X. Zhang, A. Viswanath, Y. Chumlyakov and H.J. Maier, Acta Mater. 49 (2001) p.3621.
[66] T. Duerig and K. Melton, *Diffuse yield drop and snap action in a Ni–Ti alloy*, in *MRS Proceedings*, Cambridge University Press, Boston, 1991, p.159.

Downloaded by [University of Illinois at Urbana-Champaign] at 02:30 20 May 2015

[67] V.B. Krishnan, *Low Temperature NiTiFe Shape Memory Alloys: Actuator Engineering and Investigation of Deformation Mechanisms Using In Situ Neutron Diffraction at Los Alamos National Laboratory*, University of Central Florida, Orlando, FL, 2007.
[68] T. Ezaz, J. Wang, H. Sehitoglu and H.J. Maier, Acta Mater. 61 (2013) p.67.
[69] J.C. Slater, J. Chem. Phys. 41 (1964) p.3199.
[70] F. Yang, D. Coughlin, P. Phillips, L. Yang, A. Devaraj, L. Kovarik, R. Noebe and M. Mills, Acta Mater. 61 (2013) p.3335.
[71] G. Bigelow, A. Garg, S. Padula II, D. Gaydosh and R. Noebe, Scr. Mater. 64 (2011) p.725.

Downloaded by [University of Illinois at Urbana-Champaign] at 02:30 20 May 2015